

FIGURE 3.5: COMSOL Multiphysics geometry rendering of cube shell, with Cold Spot (blue) and Hot Spot (red) connected via thin plate (yellow).

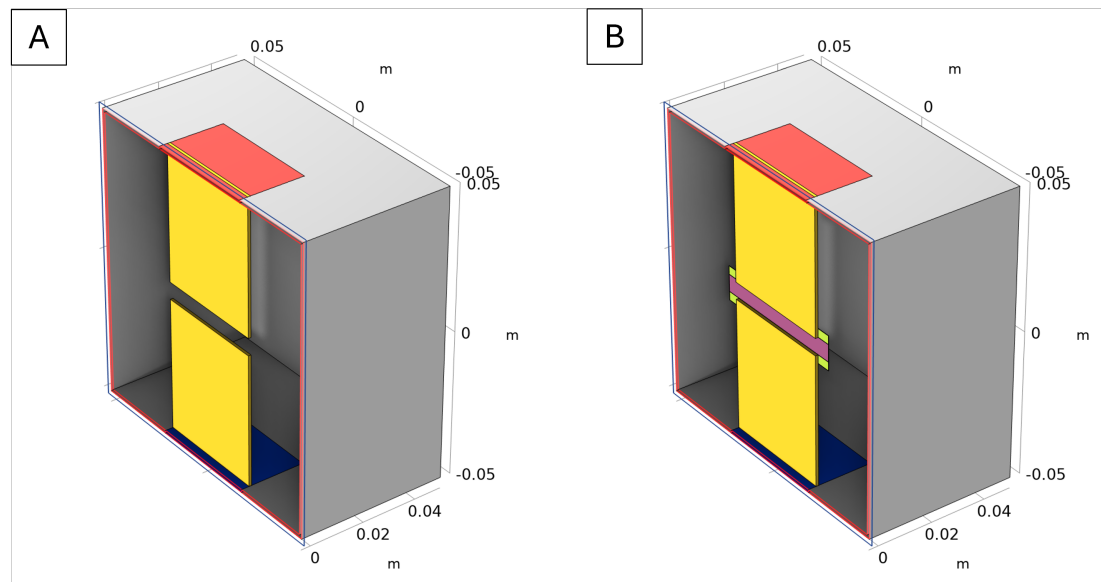


FIGURE 3.6: a) COMSOL Multiphysics geometry rendering of preliminary model with bar split in two parts. b) Final preliminary model with TEG Substitute (purple=semiconductor, green=contacts) connected via Thermal Links (yellow).

TABLE 3.2: Geometry and positioning of preliminary model in COMSOL Multi-physics.

Element	Dimensions (w x h x d) mm	Position (x/y/z) mm
Cube Shell	100 x 100 x 100 (t=1mm)	0/0/0
Hot/Cold Spots	60 x 40 x 1	0/0/ ± 49.5
Hot/Cold Thermal Links	60 x 47 x 1	0/0/ ± 29.5
TEG Substitute Contacts	60 x 3 x 0.135	0.5675/0/ ± 4.5
TEG Substitute Center	60 x 6 x 0.135	0.5675/0/0

linking TEG legs together, although are one continuous strip in this substitute model - as is the central area representing the TEG legs.

3.3.2 Material Selection

The primary concern for material selection for this model was thermal insulation of the TEG from the surrounding radiative environment, with the aim of channeling a high proportion of the radiation from the Sun and Earth into the CubeSat through the Hot Spot and out into the cold of space via the TEG Substitute and finally, the Cold Spot, on the other side. Initial simulations showed that using a material with a low thermal conductivity for the surfaces of the cube shell was crucial in order to minimise thermal energy being conducted to the Cold Spot from the rest of the structure. At first, Al 7075-T6, a commonly used aluminum alloy within CubeSats, was assigned to the cube surfaces. However, this proved to be unsuitable as the high thermal conductivity did not thermally insulate the Cold Spot causing a much smaller temperature gradient than was expected. Therefore, a carbon fiber composite with transverse fibers was selected as it is fairly resistant to conduction and is a commonly used material for space applications. As a result of switching to this material, the maximum temperature gradient increased from $\sim 10^{\circ}\text{C}$ to $\sim 100^{\circ}\text{C}$ during one orbital period.

Initially, copper was selected for the Hot/Cold Spots due to a high thermal conductivity but was replaced with Al 7075-T6 as it has a similarly high thermal conductivity, whilst being more appropriate for a structural mass of the design. To maximise absorptance of the Hot Spot, the $+z$ face boundary was assigned a CHEMGLAZE Z306 black coating. For the Hot Spot, to maximise emissivity and limit absorptance, the $-z$ face boundary was assigned a material with properties imitating that of a white thermal paint.

The Thermal Links, connecting the TEG substitute to the Hot/Cold Spots, were switched to silver from copper due to silver having an extremely high thermal conductivity. Maximising the ease of thermal flow through the central connections is highly important for achieving high temperature gradients across the TEG.

The TEG Substitute design aims to largely emulate the thermal behaviour of the real TEG with a simple architecture. The full TEG model uses silver for the contacts - as

TABLE 3.3: Table showing materials used for each geometry element of the preliminary model and their surface properties.

Element	Material	Surface Coating	α/ϵ
Cube Shell	Carbon Fiber Composite	White Paint	0.20/0.90
		Grey Paint	0.55/0.90
		Z306 Black Coating	0.90/0.95
Hot Spot	Al 7076-T6	Z306 Black Coating	0.90/0.95
Cold Spot	Al 7075-T6	White Paint	0.2/0.90
Hot/Cold Plates	Silver	None	-
TEG Substitute Contacts	Silver	None	-
TEG Substitute Center	Bismuth Telluride	None	-

were the contact strips in the substitute model. Bismuth Telluride and Antimony Telluride have similar thermal conductivities, so either could be used for the middle strip representing the TEG legs - but ultimately the former was selected and assigned.

TABLE 3.4: Table showing additional property inputs required for simulation.

Material	Surface Emissivity ϵ	Additional Values
Carbon Fiber Composite [52]	0.80	-
Al 7076-T6 [53]	0.80	$\alpha t = 23.6\text{e-}6 \text{ K}^{-1}$
Silver [54]	0.02	-
Bismuth Telluride [55]	-	$\rho = 7700 \text{ kg/m}^3$ $C_p = 154 \text{ J/kg*K}$

3.3.3 Simulation Physics Settings

With the sole concern of thermal analysis from this preliminary study, only two physics trees were used: Heat Transfer in Solids (ht) and Orbital Thermal Loads (otl). These two physics modules were linked via the heat transfer with surface-to-surface radiation multiphysics module.

Heat Transfer in Solids was active in all domains of the model and only needed two settings changed from default. The initial temperature of the model was set to -73°C as an approximate estimate of a temperature that the CubeSat would experience in this LEO environment based upon expectations of potential temperatures. Additionally, a volume reference temperature was required - setting the temperature at which there is no strain upon the model and therefore is appropriate to be an approximate mid-point temperature of those present throughout the simulation. Temperatures were observed to range from approximately -73°C to 77°C during preliminary simulations - so 2°C was set accordingly.

Orbital Thermal Loads manages the radiative interactions between surfaces, as well as the overall environment. Importantly, radiation was disabled for all surfaces in contact with another surface because conduction would be dominant and errors occurred due to opacity complexities. In reality, there may be some radiation being emitted through surfaces that are in contact, however this interaction is highly complex and would not change much of the overall thermal behaviour. Moreover, the Ray Shooting method was selected for the surface-to-surface radiation method as opposed to the default Hemicube option. Ray Shooting is more suitable for more complex geometries and so performed better once the preliminary model was completed with objects inside the geometry, making view factors more complicated.

TABLE 3.5: COMSOL Multiphysics settings for Orbital Thermal Loads - Planet Properties and Orbital Parameters.

Physics Setting	Parameter	Selected Option	Value
Radiative Properties	Albedo	User-defined Distribution	0.3
Radiative Properties	Planet Radiative Flux	User-defined for each band	Solar = 0 W/m ² Ambient = 225 W/m ²
Orbital Parameters	Orbit Type & Elements	Elliptical	a = 6771 [km] e = 0 i = 51 [deg]
Orbital Parameters	Ascending Node	Longitude of Ascending Node	$\Omega = 10$ [deg] $\omega = 315$ [deg] $\nu_0 = 0$ [deg]

In order to accurately simulate the correct representative thermal environment in LEO, radiative properties must be set to configure the albedo and IR radiation sources originating from Earth. These radiation sources incident on the spacecraft will vary across the Earth's surface due to atmospheric and geological features and so widely used average values were used [56]. With regards to direct solar radiation, all default settings were used and the primary axis (+z-axis) were orientated in the direction of the sun under spacecraft orientation settings. The secondary axis was designated to the +x-axis and orientated in the velocity direction. This configuration of settings ensured that the solar radiation would hit the +z face of the model at a perpendicular angle - directing the maximum amount of solar radiation to the conductive area on that side.

Finally, diffuse surface nodes were created for each unique material in which the boundary selection was filled with boundaries pertaining to objects assigned to that material. The surface emissivity was defined on each side of the boundary to match that of the material used, with the ambient temperature changed to -269°C. All other settings were left as default.

3.4 1U CubeSat Model

3.4.1 3D CAD Model

Building off of the preliminary model that outlined the structural system that would be used for this investigation, a 1U CubeSat model was imported into Solidworks from existing CAD files and modified to match the general concept of the preliminary model. An assembly of a realistic 1U CubeSat was used as the basis for my design upon which five unique parts were added.

Five additional parts were created within Solidworks and added to the existing CAD model in order to form the top and bottom panels with the Hot/Cold Spots and internal TEG Substitute structure and Thermal Links. These parts were joined to the existing model using the Mate feature in Solidworks. The CAD file was then imported into COMSOL Multiphysics.

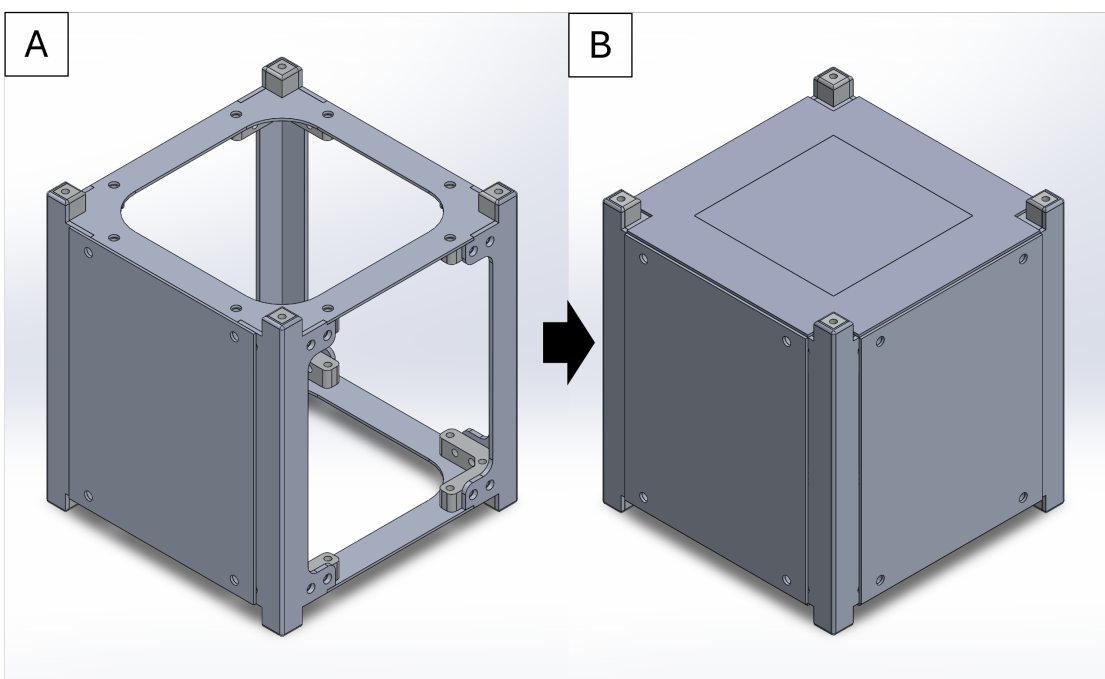


FIGURE 3.7: Initial and completed versions of 3D CubeSat Model. a) Imported CAD Model assembly. b) Completed CAD Model.

3.4.2 Material Selection

In order to progress this model to become a more realistic representation of a CubeSat, the side panels were changed to a commonly used material: PCB (FR4). Even though carbon composites are used in CubeSats, side panels are usually made from PCB and solar panels. However, Al 7075-T6 was used for the rails and frame supporting the top, bottom and side panels - including the rails, joining brackets and Hot/Cold Spots. The

low thermal conductivity of FR4 is consistent with the carbon composite used in the preliminary model and still minimises conduction through the surface of the CubeSat.

Considering the Thermal Links providing the heat transmission between the TEG and the face of the CubeSat, the material used for these elements would greatly impact the temperatures of the TEG. Silver is an excellent thermal conductor and was selected for the Thermal Links to maximise heat transport through the system. However, it is not suitable, in reality, to form a significant part of the structure of the payload due to it being inherently weak and heavy. Alternatively, Al 7075-T6 is the obvious choice in terms of ease of fabrication, weight and structural stability, but does suffer a large decrease in conductivity when compared to silver. Fortunately, when comparing the overall temperature gradient from simulations performed using either material, aluminium led to a decrease of only 2 degrees. From this comparative study, aluminium was deemed a good enough conductor for the thermal loads present in this design. Perhaps if the heat flux was increased significantly, then a better thermal conductor should be considered. A further comparison of the three candidate materials for the Thermal Links can be seen below in Table 3.6. Al 7075-T6 performed well enough as a conductor, as well as, outperforming copper and silver in density and strength properties. Considering all these factors, Al 7075-T6 was chosen as the final material selection for the Thermal Links. All other material selections were kept from the preliminary model.

TABLE 3.6: Comparison of suitability of materials used for Thermal Links. All values obtained from COMSOL Multiphysics library at 300K.

Material	Young's Modulus (GPa)	Density (kg/m ³)	Thermal Conductivity (W/mK)	Cost	Ease of Fabrication
Copper	127	8936	388	Low	Easy
Silver	80.8	10500	429	Medium	Easy
Al 7075-T6	70.8	2718	168	Low	Medium

3.4.3 Simulation Physics Settings

The geometry for the 1U CubeSat model is much more complex than that of the preliminary model and so some settings must be altered for the radiation to function effectively. All faces that directly contact the face of another object have been disabled under Orbital Thermal Loads once again to avoid errors. Also, only large faces on objects have radiation enabled, with any small faces being disabled in order to limit the complexity of the simulation without affecting the result deleteriously. Furthermore, radiation has been disabled for the entire TEG as it is comprised of many exceedingly thin and

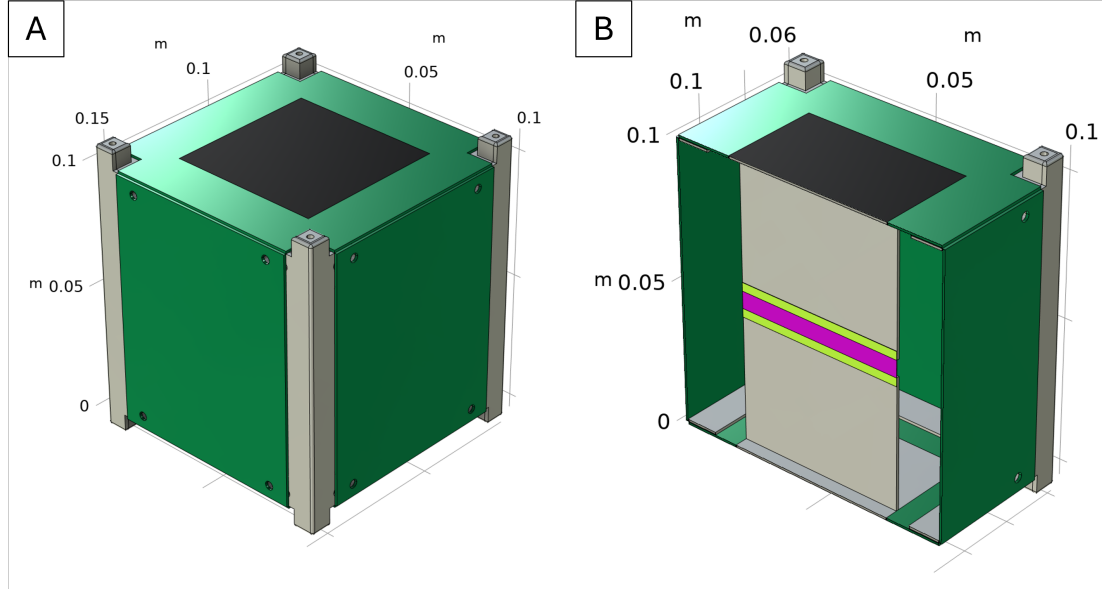


FIGURE 3.8: 1U CubeSat Model in COMSOL Multiphysics. Green = PCB/FR4, Black = Z306 Thermal Paint, Grey = Al 7075-T6, Lime Green = Silver, Magenta = Bi₂Te₃.

small faces. Again, disabling these radiation processes will not affect the overall thermal dynamics significantly as thermal transfer by emission will be low in comparison to thermal transfer by conduction.

3.5 Combined Model

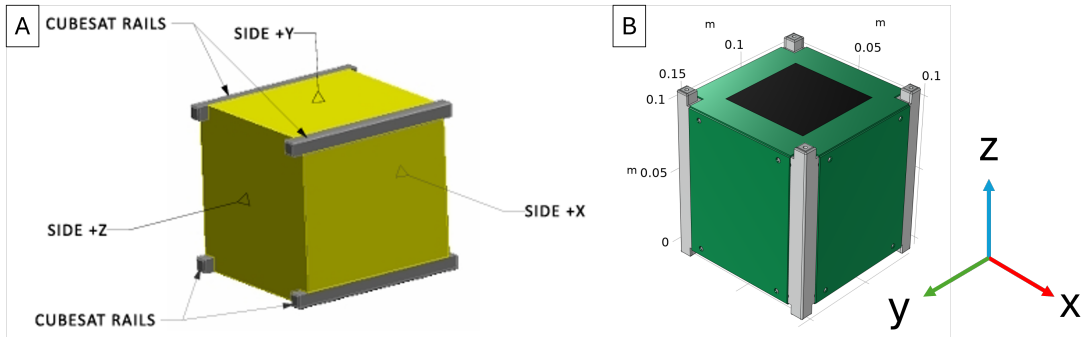


FIGURE 3.9: a) 1U CubeSat axis specification from Cal Poly [11]. b) Axis orientation of Combined Model.

All the previous iterations of designing this system culminate in this final design model: a 1U CubeSat Model connected to a thermoelectric generator capable of producing voltages. Creating the model simply required removing the TEG Substitute from the 1U CubeSat model and replacing it with the TEG model ($L = 60 \text{ mm}$).

In accordance with official CubeSat design specifications [11], the axis orientation is aligned as shown in Fig 3.9.

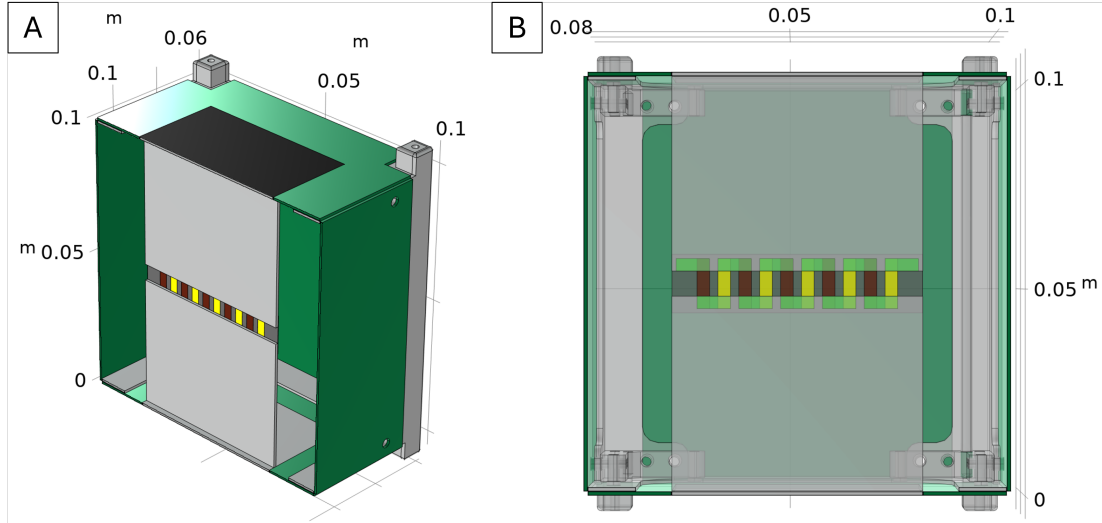


FIGURE 3.10: Final Combined Model of the 1U CubeSat housing TEG payload. a) Cross section of Combined Model. b) Transparent view of cross sectioned Combined Model (xz view).

3.5.1 Simulation Physics Settings

Electric Currents and Electrical Circuits modules were set up to match the sole TEG simulation, along with the Multiphysics interaction modules: Thermoelectric Effect and Electromagnetic Heating. The domains pertaining to the TEG itself were only selected for these electrical modules to be active since there would be no significant electrical activity outside of the TEG. In addition, the thermal modules were set up to be almost identical to the 1U CubeSat model with Heat Transfer in Solids being active over all domains, whilst emissive radiation being enabled only for large faces.

Upon inspection of the temperature plots produced from the preliminary model and 1U CubeSat model simulations, the inconsistency of starting and end temperatures of the TEG were cause for concern. Due to the cyclical and unchanging nature of the orbital thermal loads experienced by the structure, there should be a cyclical pattern to the temperatures of the spacecraft. Therefore, the temperature at start and end of one orbit should be similar. From this, it was concluded that the initial temperature condition of -73°C was impacting the validity of the results. After running the simulation on the 1U CubeSat Model for five orbital periods, a pattern was produced and starting temperatures of -2°C and 58°C on the cold and hot side of the TEG, respectively, were established from the plot. Applying accurate initial conditions to the whole model is practically impossible as the whole spacecraft will have varying temperatures throughout the structure. Therefore, with the intention of helping the model reach an accurate initial condition quickly, three initial value sub nodes were created in COMSOL. The first sub node applied to the Hot Spot and Hot Thermal Link (+z direction from TEG), was set to 58°C. A second sub node applied to the Cold Spot and Cold Thermal Link (-z direction from TEG), was set to -2°C. The remaining domains of the model were set to

7°C, a middle ground between the colder temperatures of the PCB faces and the hotter temperatures of the aluminium frame.

3.5.2 Mesh Settings

A physics-controlled mesh at a *Finer* element size was found to be the optimal settings giving the fewest elements with bad quality. Out of 83 million elements, only two elements were of bad quality (near zero skewness).

3.5.3 Computation Method

Two solution steps were computed - namely Orbital Thermal Loads and Orbital Temperature. These solvers evaluated the thermal environment and temperature of the model over one orbital period at intervals of 0.05 periods, resulting in 20 steps. The file was submitted to the High Performance Computing system at the University of Southampton (Iridis 6).

Values for the current flowing through each terminal were obtained from the *Global Evaluation Table* under *Derived Values in Results*. Evaluating for the following expressions gave data for current flowing through each terminal at every time step: *ec.I0_1* & *ec.I0_2*.

Chapter 4

Results

4.1 Thermoelectric Generator

The following data was gathered from exposing the TEG to a 100°C gradient and capturing a snapshot of the electric potential and temperature throughout the device under this condition. This was a simulation validating the functionality of the model by itself, without any structure around it.

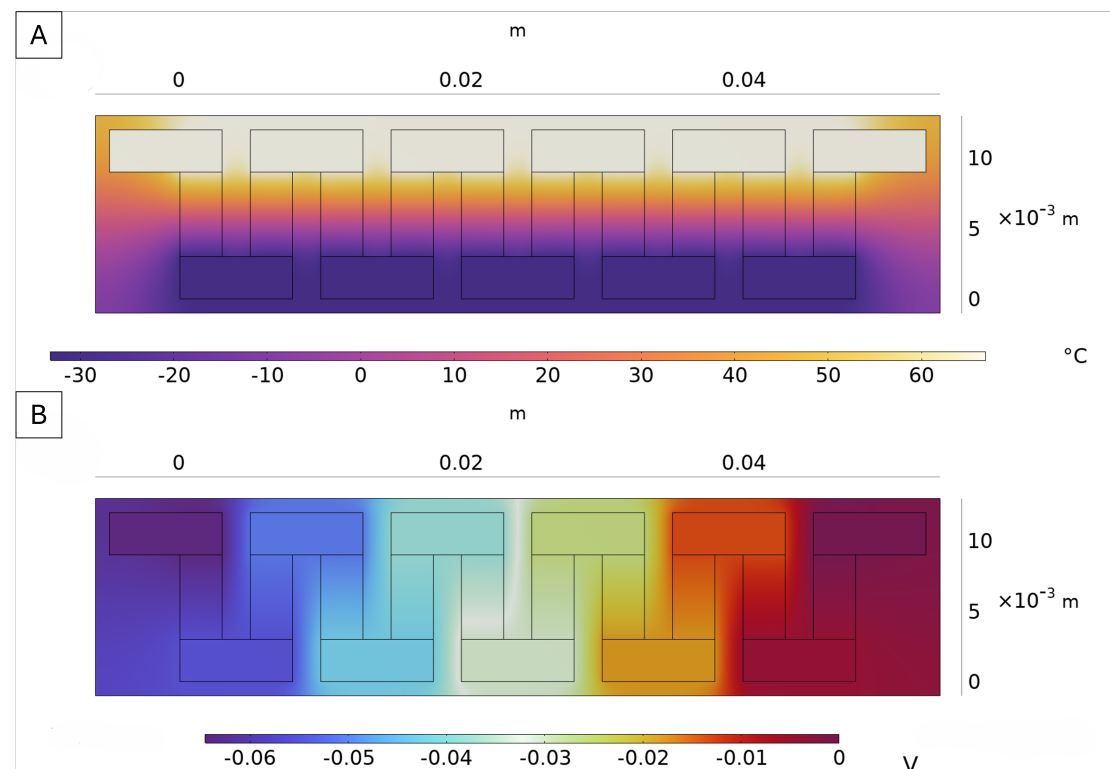


FIGURE 4.1: Temperature and electric potential distribution maps from stationary study of TEG at 100°C gradient. a) Temperature distribution map of TEG. b) Electric potential distribution map of TEG.

4.2 Preliminary Model

The following plot shows data retrieved from the TEG Substitute over one orbital period at 400km altitude and 51° inclination (ISS orbit). The difference in these temperatures is plotted simultaneously, namely "Delta-T".

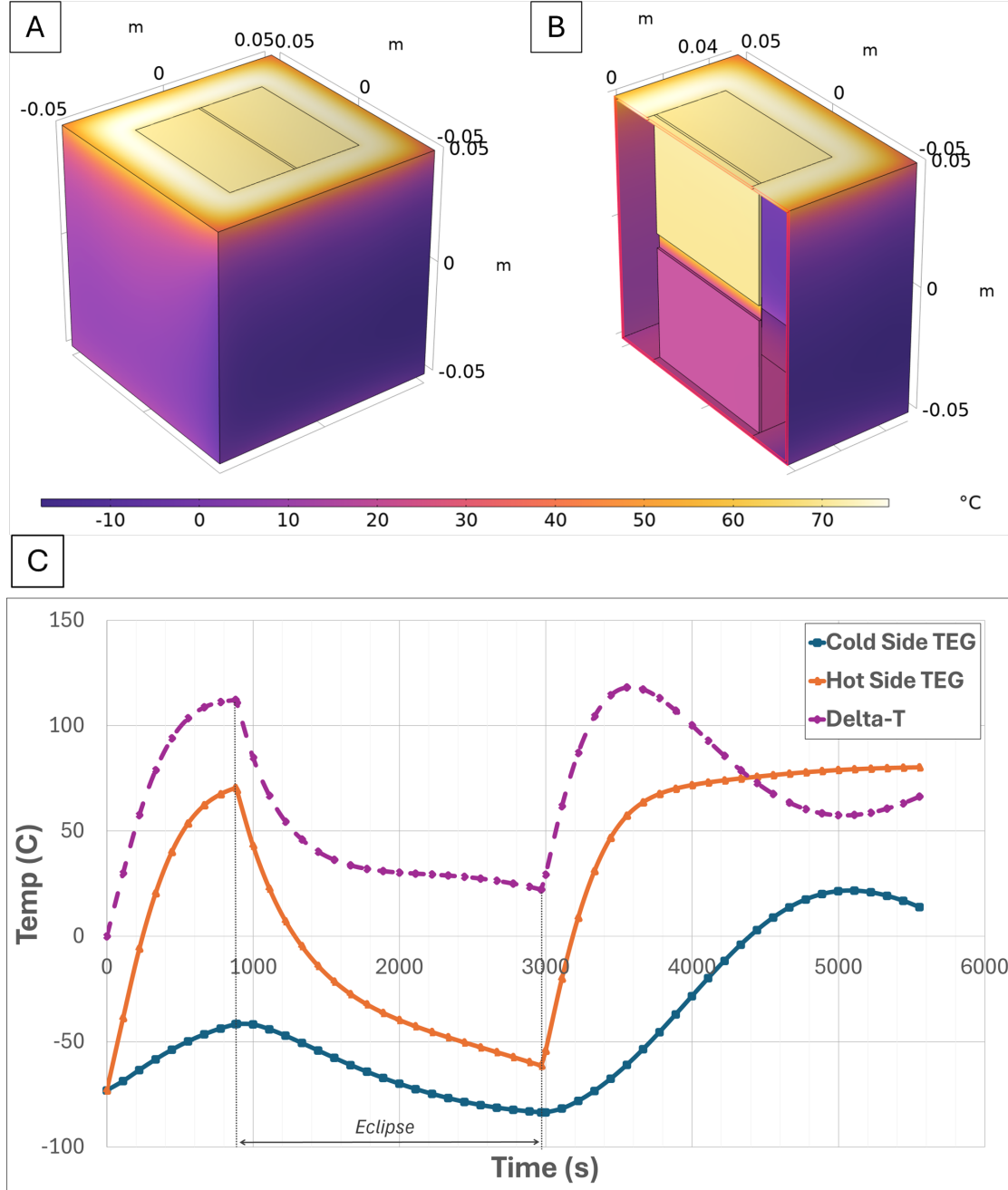


FIGURE 4.2: Data describing thermal behaviour of preliminary model. a) Temperature distribution map of exterior. b) Temperature distribution map with cross-section. c) Plot showing temperature data from TEG Substitute.

4.3 1U CubeSat Model

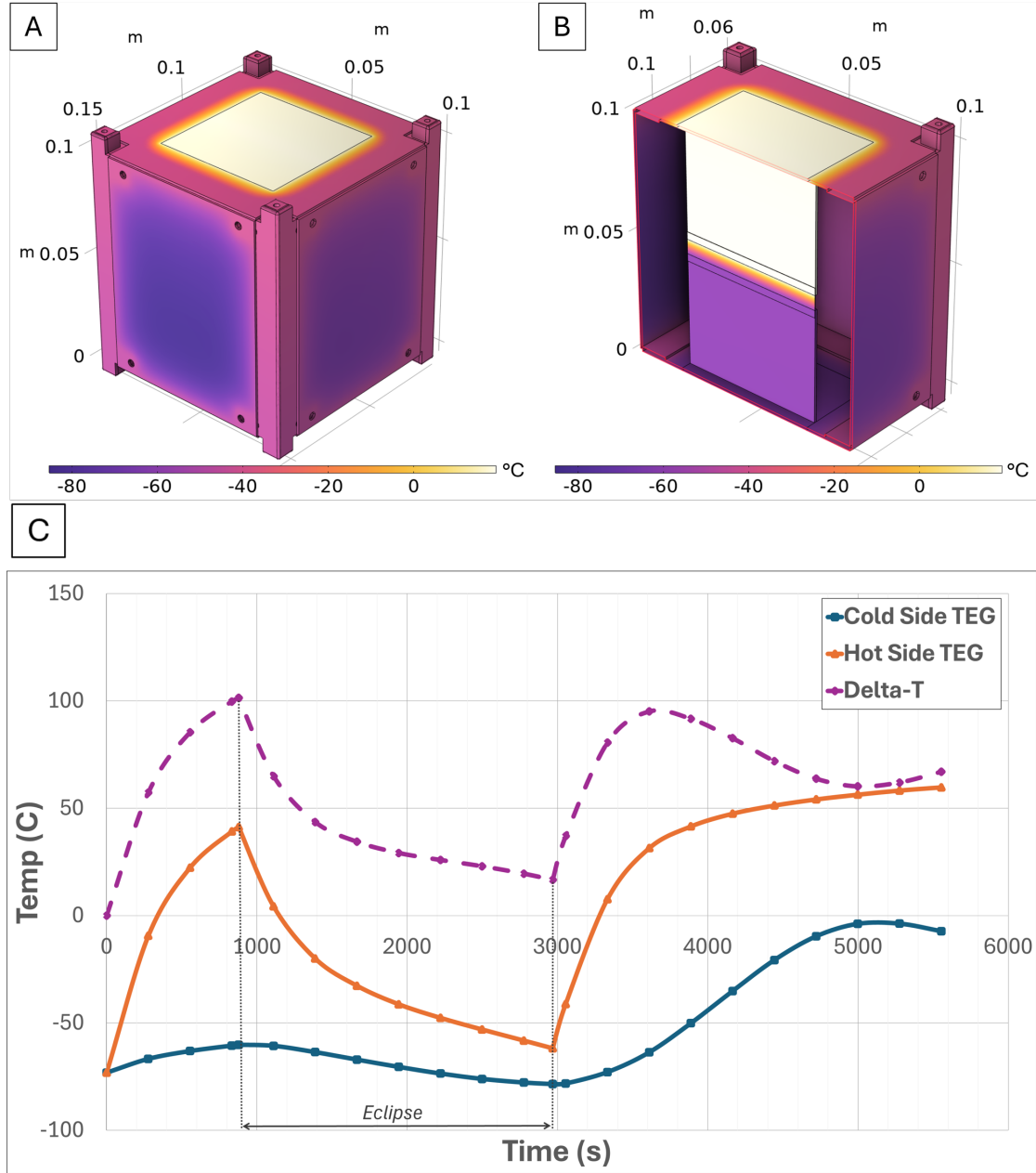


FIGURE 4.3: Data describing thermal behaviour of 1U CubeSat Model. a) Temperature distribution map of exterior. b) Temperature distribution map with cross-section. c) Plot showing temperature data from TEG Substitute.

4.3.1 Refinement studies

The following plots show results obtained from refinement studies whereby the Thermal Link material was varied, and the number of orbits was increased to five, respectively. These simulations were set up in an identical manner to the 1U CubeSat Model simulations, except for the parameters central to their study.

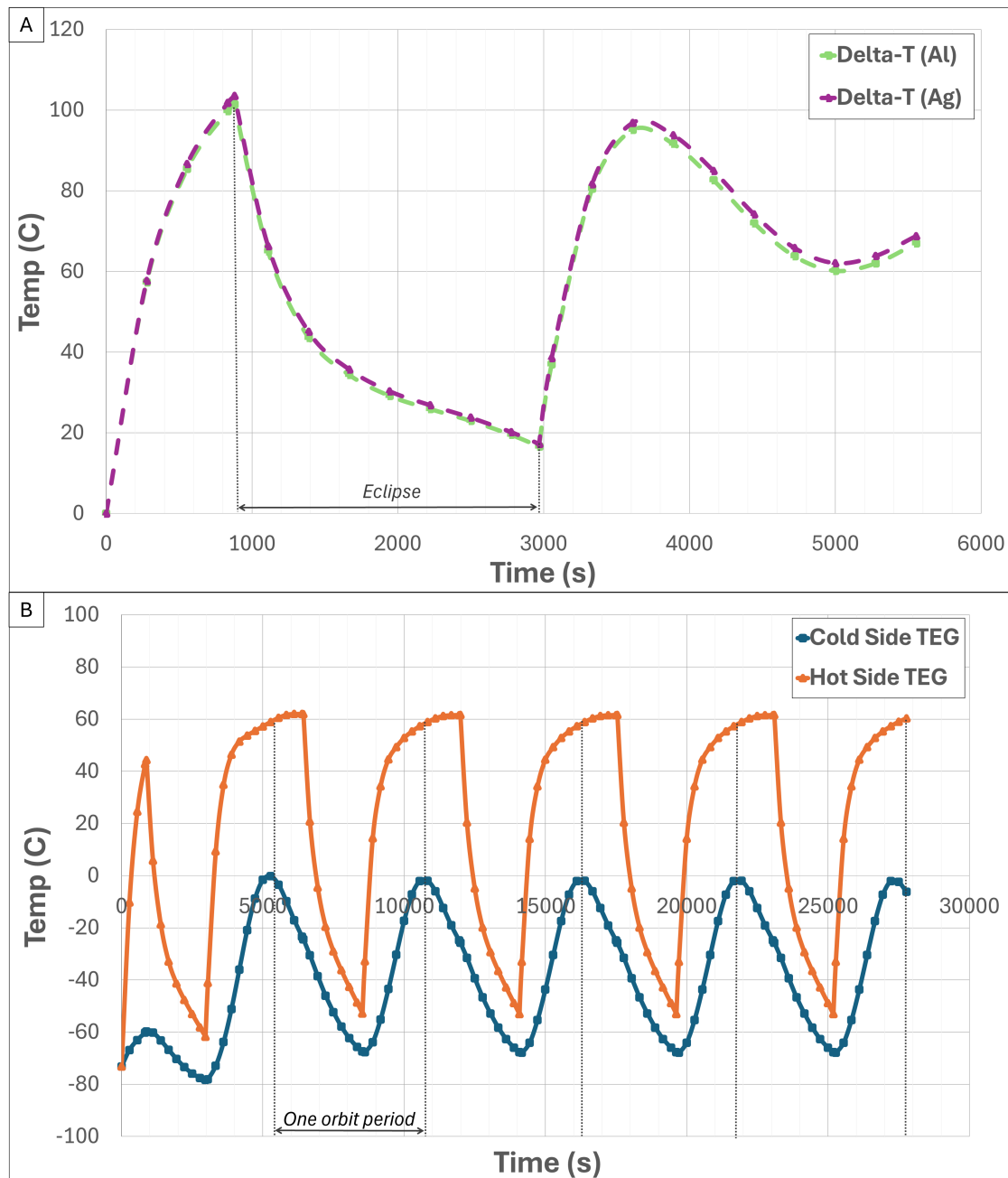


FIGURE 4.4: a) Plot comparing temperature gradient over TEG Substitute for aluminum and silver used for Thermal Links. b) Simulation run over five orbital periods to refine temperature boundary conditions.

4.4 Combined Model

The following results include a table listing all the relevant thermal and electrical values obtained from each scenario of the parameter study. Fig 4.5 shows an example visualisation of the how the heat travels through the whole system and a snapshot of electric potential distribution over the TEG. Fig 4.6 shows plotted data taken from the best performing scenario ($\alpha = 0.55$) to show the output thermal and electrical behaviour of the TEG over one orbital period. Only plots from the one scenario are presented because the data from all three studies do not deviate from each other enough to be visible.

It should be noted that the values pertaining to current were extracted from terminal 2 of the TEG and have a negative value. Only absolute values have been presented here.

TABLE 4.1: Average and peak thermal and electrical values from parameter study of three distinct exterior absorptances.

	$\alpha = 0.2$ (White)	$\alpha = 0.55$ (Grey)	$\alpha = 0.84$ (Black)
Peak Delta-T (°C)	106.2	106.7	104.9
Average Delta-T (°C)	60.7	60.9	60.1
Peak Voltage (mV)	57.0	57.2	56.2
Average Voltage (mV)	33.2	33.3	32.9
Peak Current (μ A)	57.0	57.2	56.2
Average Current (μ A)	33.0	33.1	32.6
Peak Power (μ W)	3.25	3.27	3.16
Average Power (μ W)	1.39	1.40	1.36

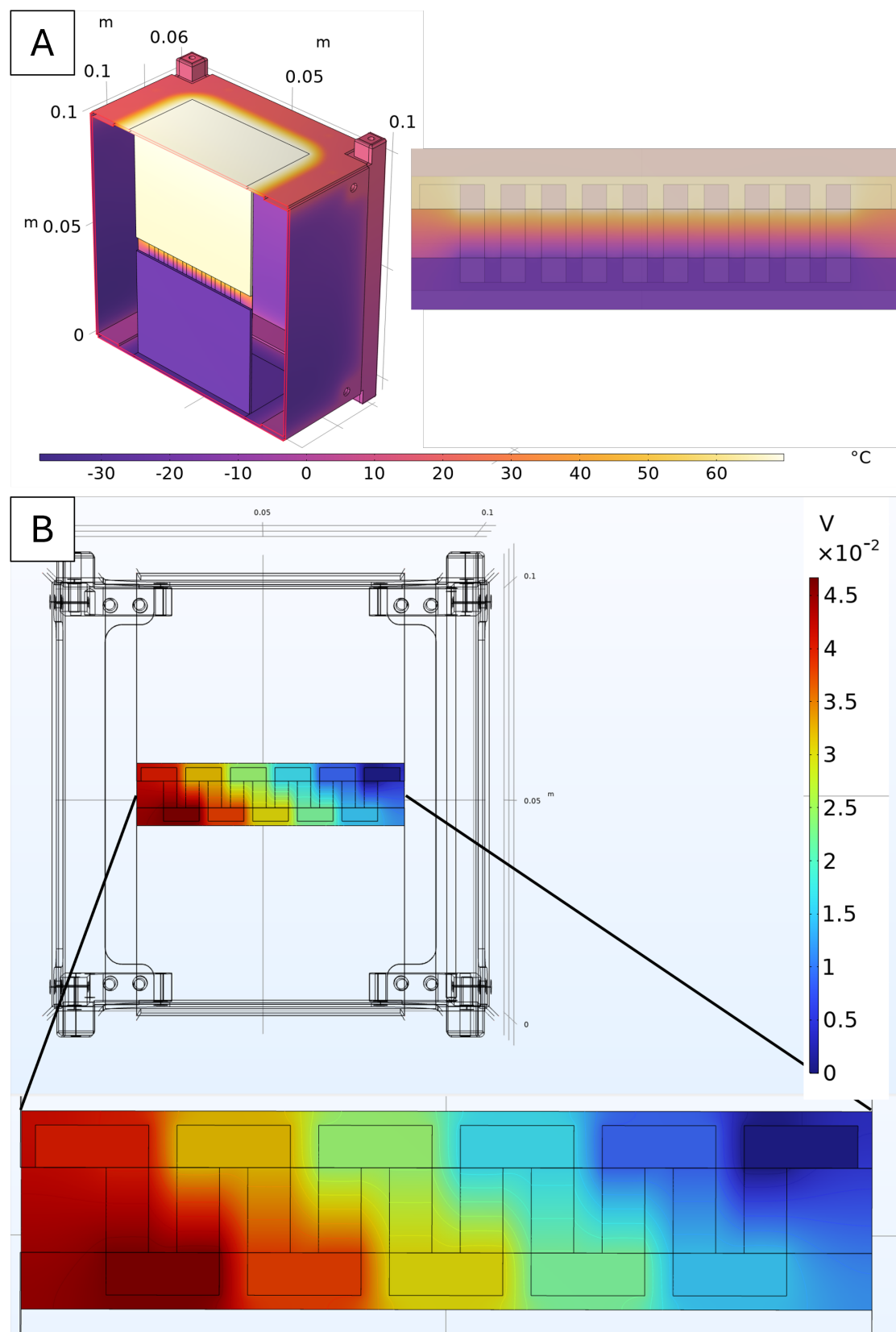


FIGURE 4.5: Visualisations of thermal and electrical distribution. a) Temperature heatmap over combined model including TEG. b) Electric potential distribution over TEG.

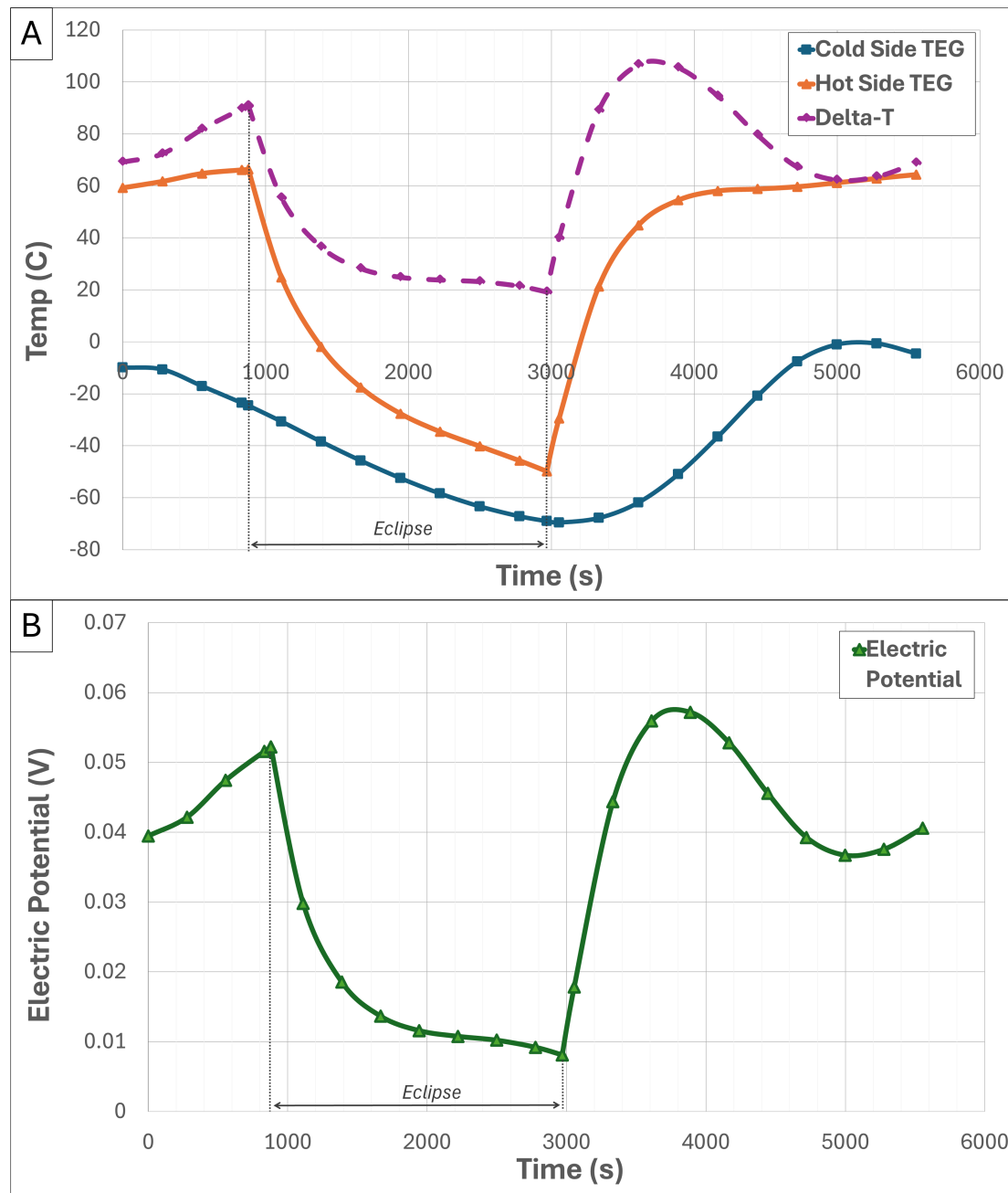


FIGURE 4.6: Plots from $\alpha = 0.2$ Combined Model simulation. a) Thermal behaviour of TEG over one orbital period. b) Electric potential generated over one orbital period.

Chapter 5

Discussion

5.1 Effectiveness in Orbital Thermal Environment

The chief intention of this research is to offer some novel insights into the thermal and electrical characteristic behaviours that thermoelectric generators may exhibit in orbit. Of primary concern is the temperature gradient (ΔT), which was shown to exceed 100°C for \sim 10 minutes, whilst averaging 60-61°C over the 90 minute orbital period.

The general behaviour can be split into five phases. The first phase consists of a steady rise from 70 - 90°C over 15 minutes, due to heating from solar radiation, followed by an eclipse period, lasting 30 minutes; constituting the second phase. A sharp decline in ΔT occurs for \sim 7 minutes, as the source of solar radiation is cut off, rapidly cooling the Hot Spot of the CubeSat. After falling from $\Delta T = 90^\circ\text{C}$ to 40°C , the whole system cools at similar rates leading to a gentle decrease to 20°C . Upon exiting the shadow of Earth, phase 3 sees a rapid rise from solar heating until the -z face of the CubeSat starts to become exposed to the Earth's IR and reflected radiation (albedo). Phase 4 describes a 45°C decrease - explained by thermal energy being added to the system through the cold side of the CubeSat due to Earth's radiative sources. Bounded by the highest peak and the subsequent trough, at which point the z-axis of the spacecraft is perpendicular to the termination line over Earth. Here, the view factor of Earth from the -z face has reached a maximum; after which phase 5 commences. Phase 5 is characteristically similar to phase 1, with a steady increase in ΔT as the heating from Earth weakens.

It is difficult to attempt an assessment of the potential effectiveness of this technology in an orbital environment from the results produced. The power generated is small, but not insignificant; a comparison can only be made to the investigation undertaken by Curry et al. [10], as mentioned in chapter two. An array of sixteen full-sized models were used to charge a $6600 \mu\text{F}$ capacitor at $13.6 \mu\text{W}$, in 25 minute intervals, however these TEGs were full sized (ten leg pairs) and had a optimised TEG leg length (6 mm

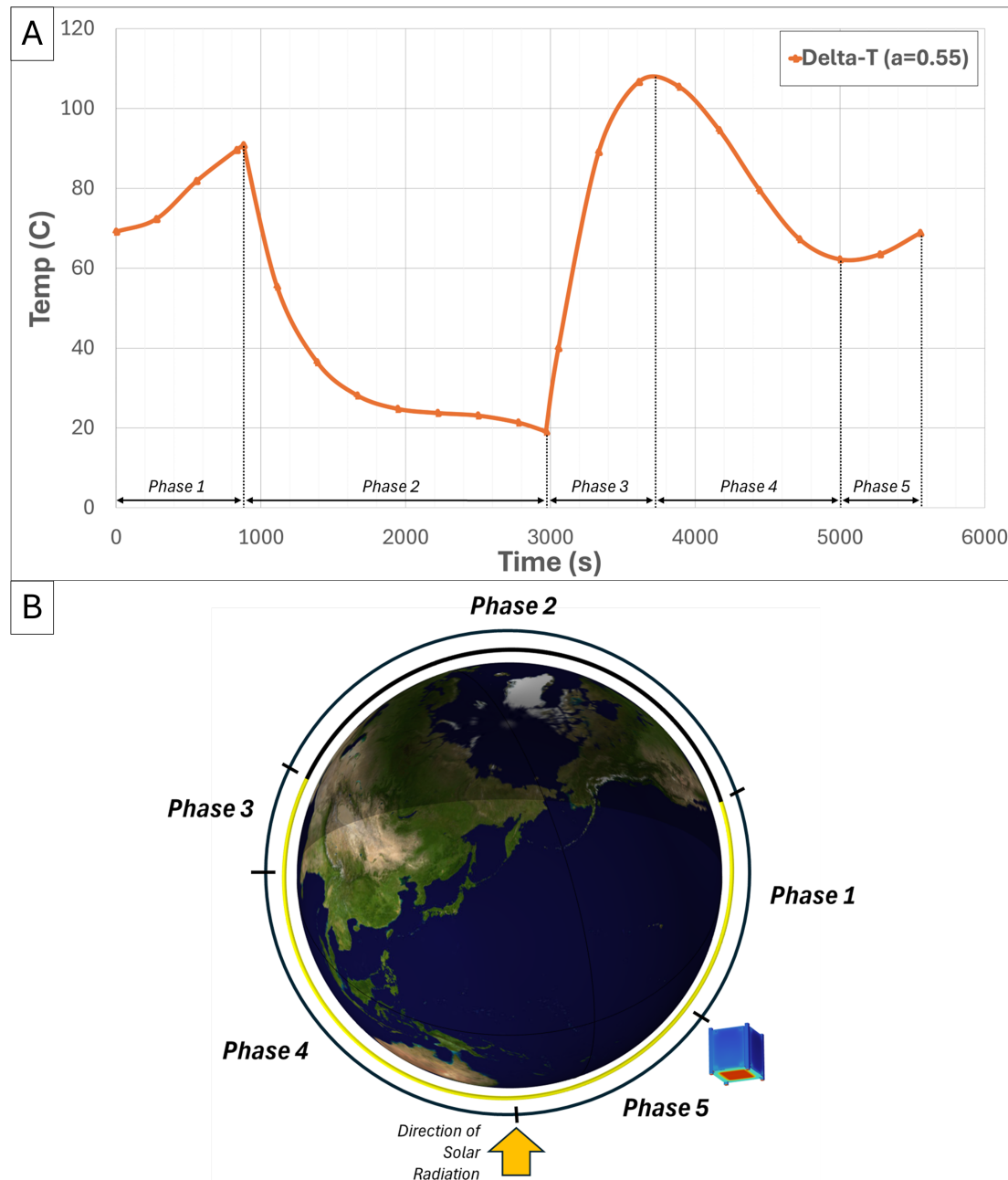


FIGURE 5.1: Characteristic thermal behaviour of TEG over orbital period. a) Plot showing ΔT over TEG. b) Orbit visualisation, including phases of thermal behaviour.

instead of 12 mm). Taking into account the differences in size, number of TEGs and optimisation: simulation results show an average output of $1.40 \mu\text{W}$ from 5 leg pairs - approximately one-tenth of the power output of the sixteen TEG array with 160 leg pairs. Importantly, the 16 f-TEGs performed with $\Delta T = 25K$ - less than half of the average thermal gradient found to be present for the Combined Model simulations.

If the same experiment, performed by Curry et al., were to be set up in an orbital thermal environment, the output power would undoubtedly increase, possibly by twice the magnitude. Also, it should be considered that a larger CubeSat, with larger area for thermal energy collection/dissipation, would most likely increase the hot side of the TEG and therefore increase the thermal gradient. A CubeSat of a greater volume than 1U would most likely be required to fit multiple TEGs inside. Therefore, with a larger CubeSat to house an array of f-TEGs, the average power output should increase significantly.

5.2 Parameter Study Findings

The results produced from the three comparative studies, whereby the absorptance of the exterior CubeSat surface were varied, showed little change of the TEG's behaviour. Surprisingly, the largest peak values for delta-T and voltage were yielded from the grey paint ($\alpha = 0.55$), with 106.7°C and 57.2 mV , respectively. From studying the preliminary model and changing the materials for the CubeSat faces, it became apparent that conduction through these surfaces should be minimised in order to insulate the cold side of the TEG. Using this logic, it would be reasonable to suggest the absorptance of the exterior surfaces and the overall absorption of thermal radiation should be positively correlated - leading to the expectation that white paint would cause the highest thermal gradient. However, lowest absorptance ($\alpha = 0.2$) led to a slightly lower average delta-t of 60.7°C , compared to 60.9°C when using $\alpha = 0.55$. The worst performer was the black paint ($\alpha = 0.84$) with an average delta-t of 60.1°C . The reason behind this slight and unexpected increase in performance is unknown and should be a focus for investigation on future tests. In particular, I recommend that the surface properties for the hot and cold spots of the CubeSat faces be varied, in order to observe the effect on the TEG temperature gradient. When applied to EVA suits, this would direct decisions with regards to the surface colour and properties of the exterior layer of the garment.

Overall, this parameter study showed that the absorptance of the exterior surfaces of the CubeSat do not significantly impact the thermal behaviour of the TEG and therefore the performance is relatively unaffected. However, the small variations in average temperature gradients across the TEG, between the three scenarios, would expectedly increase as the model is scaled up due to the larger surface area inflating the role of surface properties in thermal dynamics.

Designers of future investigations, integrating TEGs with CubeSats, would benefit from this knowledge as usually solar panels are attached to the outside. From this study, it is advisable that materials with low thermal conductivity, such as PCB and high emissivity are used on the exterior, although absorptance is not largely significant in this consideration, unless perhaps the CubeSat is scaled up significantly.

5.3 NASA Human-Rating Certification

If thermoelectric generators are to be deemed effective and suitable for use in space, it will be essential to determine whether they are safe enough. NASA has developed a useful certification procedure for this purpose, laid out in various documents such as - NASA-STD-8719.29 (Technical Requirements for Human-Rating), and NASA-STD-3001 (Human System Standards) [57]. All space systems to be used or interacted with by humans must be shown to meet the criteria, in the following hierachal order:

1. **Fundamental System Needs** - Meeting minimum structural requirements for a crew member to be contained within.
2. **Basic Human Needs and Life Support** - Meeting human physiological requirements.
3. **Safety, Security and Vehicle Operations** - Meeting safety requirements beyond raw survival (e.g. safe flight, navigation, abort).
4. **Human and Vehicle Maintenance** - Allows crew to monitor, maintain and repair system.
5. **Enabling and Optimizing Human and Mission Performance** - Maximising performance, efficiency and optimisation (Not required for human-rating).

Once integrated into an EVA suit, the TEG energy harvesting system must be proven to be safe and effective for human use. Of primary concern is the introduction of hazards with new electrical systems. No single-point failure can be allowed to risk a crew member and so, the possibility of fire, shocks, suit-breach and other hazards must be evaluated. Additionally, the suit's internal/external environment must be preserved, as well as mobility and thermal comfort.

Crucially, the issue of thermal control must be evaluated because this system handles thermal loads, which will be added to total thermal energy of the EMU. Obvious effects of this are the increased temperature of the internal environment leading to uncomfortable or dangerous temperatures for the user and/or increased load for the cooling

system. As seen in Fig 4.6a, the cold side of the TEG did not appear to undergo vigorous heating and followed a noticeably gentler heating/cooling cycle when compared to the hot side. In fact, the cold side never exceeded 0°C (see also Fig 4.4b), even when the hot side was at 60°C. This may suggest that enough thermal energy is converted into electrical energy for the system for the increased thermal load to not cause a major safety concern. However, this suggestion can only be validated by further tests being performed with the cold side being regulated to stay at external body temperature ($\sim 36^\circ\text{C}$). In fact, in order to maximise the power generation from the temperature gradient between the body and the orbital thermal environment, I recommend configuring two TEGs to simultaneously take advantage of the cold and hot side of the CubeSat.

Furthermore, the effects of this rigorous testing process would provide clarity on the configuration of the energy harvesting system, in particular the location of the cold side of the TEG, in relation to the skin of the astronaut. The cold side contacts of the TEGs may be safe enough to be present on the inner most layer of the EMU garment - allowing for a close connection to the heat source, perhaps strengthening the temperature gradient. Or it may only be permitted to be nested within one of the exterior layers of the garment. In any case, the EVA suit is a highly complicated system with many subsystems integrated in a small space and therefore, not only will the safety of the astronaut be paramount in further consideration, but also, the effect of introducing this novel system on the function of the other subsystems.

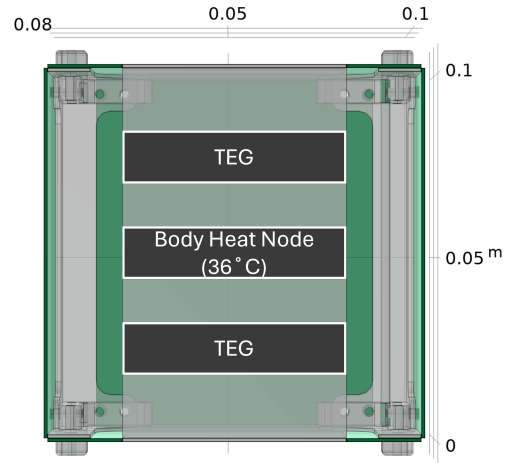


FIGURE 5.2: Proposed configuration of future investigation using two TEGs connected to a heating module emulating body heat.

Chapter 6

Conclusions

This novel investigation has successfully characterised the thermal and electrical behaviour for a thermoelectric generator, when operating under a representative thermal environment commonly seen during EVAs. Overall, the temperatures generated by a 1U CubeSat configuration are strong enough to suggest TEG operation would be effective in orbit. The operating temperature gradients for terrestrial uses are much lower and there is plenty of scope to increase TEG temperature gradients in space. An array of TEGs within a larger spacecraft, using a similar design to this investigation, would likely produce greater performance values. However, the orbital thermal environment was specifically chosen to reflect that of the ISS, and due to the upcoming decommissioning of the ISS, it would be useful to evaluate the characteristic behaviour for different orbits. The results showed that the behaviour is dependent upon the view factor of the -z face to Earth - a factor that will change depending on orbital parameters, namely inclination.

The temperature gradient, ΔT , exhibits a pattern over an orbital period that will likely sustain through all configurations of spacecraft following the same orbit. This behaviour is described by the five phases - consisting of three rises and two falls. Although, phases one and five can be combined as they are two halves of the same rise, split by the starting position of the spacecraft. Adjusting the starting true anomaly of the spacecraft to the start of phase five would optimise this analysis. Furthermore, a key value of $\Delta T = 100^\circ\text{C}$ was shown to be exceeded, whilst an average of $\Delta T = 60^\circ\text{C}$ sustained throughout the orbital period. These values could be increased with a further iteration of the experimental design proposed by this research, specifically through the use of two TEGs simultaneously capturing a thermal gradient from a common body temperature node against the hot and cold sides of the CubeSat. In contrast, this configuration would produce more power, than the Combined Model, whilst in the eclipse period, and is useful as it reflects a possible positioning upon integrating this technology into an EVA suit.

From the parameter study, it can be seen that surface properties were shown to have little effect when varied over the exterior of the model. These effects would likely increase with larger spacecrafts as the 1U volume is small and the contribution of surface properties to thermal dynamics scales with surface area. Expect larger structures to be slower to reach thermal equilibrium and stronger temperature gradients due to larger areas for dissipation, absorption and conduction. Lastly, further investigations should vary surface properties of Hot and Cold Spots to obtain a range of temperatures - implicating surface properties, such as colour, for EVA suits.

Utilising bio-thermoelectric energy harvesting in space is possible as this research has shown that there is likely to be sufficient temperature gradients for TEGs to function effectively. Limited by the inherently low levels of power generation, this technology would need a numerous array of f-TEGs to be able to provide supplementary power to a system such as an EVA suit. With an estimated power consumption of up to 100 W, there is much advancement in capabilities needed before bio-thermoelectric power would be able to replace even a portion of current battery power supplies. Additionally, experimental data needs to be gathered to investigate how f-TEGs cope with the features of an orbital environment: micro-g, vacuum, radiation and high energy particles. Calculating changes in key performance parameters, for example, ZT, ω_{max} and η_{max} , between terrestrial and orbital environments may offer a key numerical comparative analysis. Beyond meeting fundamental requirements of the environment, other operational issues, such as thermal cycling and bending cycling, will need to be studied. Fortunately, f-TEGs benefit from increasing research in the medical science field as wearable devices are being developed for wider use. Solutions to mitigate performance degradation of f-TEGs caused by thermal and bending cycling would be a worthwhile consideration when manufacturing f-TEGs for use in space due to the costly nature of delivering payloads into orbit.

To conclude, thermoelectric generators show potential for use in space because of the presence of useful temperature gradients, shown by this novel study. The characterisation of the TEG in a representative thermal environment should give future investigations a platform to gain further insight into the application of this technology with regards to Extra Vehicular Activities. However, many more factors must be considered and analysed in order to advance this technology to a higher readiness level to prove that it is truly effective - not to mention the rigorous safety requirements set out by NASA's human-rating certification. Among an accelerating global space economy, innovative solutions, such as bio-thermoelectric power, may offer increased capabilities and practical support required upon the increasingly ambitious missions ahead of humanity.

References

- [1] E. Mathieu, P. Rosado, and M. Roser, "Space exploration and satellites," *Our World in Data*, 2022, <https://ourworldindata.org/space-exploration-satellites>.
- [2] "Astronaut bruce mccandless on first-ever untethered spacewalk," 12 2017. [Online]. Available: <https://www.nasa.gov/image-article/astronaut-bruce-mccandless-first-ever-untethered-spacewalk-3/>
- [3] S. P. Russell, M. A. Elder, A. G. Williams, and J. Dembeck, "The extravehicular maneuvering unit's new long life battery and lithium ion battery charger," American Institute of Aeronautics and Astronautics, Tech. Rep., 2010.
- [4] "Portrait – full-lenth – mercury astronaut l. gordon cooper, jr. – spacesuit," 5 1963. [Online]. Available: <https://www.nasa.gov/image-detail/amf-s63-01755/>
- [5] "Gemini iv," 1967. [Online]. Available: <https://archive.org/details/S67-24267>
- [6] S. M. Group, "Science museum group. apollo 17 space suit replica." [Online]. Available: <https://collection.science museumgroup.org.uk/objects/co8645938/apollo-17-space-suit-replica>.
- [7] "Axiom axemu full," 7 2023. [Online]. Available: https://brandfolder.com/axiomspace/newsroom?o=OR&q=custom_fields.Program.strict%3A%28%22Axiom+Suit%22%29
- [8] "Nasa engineering & safety center technical update," NASA, Tech. Rep., 2015.
- [9] Y. Liu, J. R. Riba, M. Moreno-Eguilaz, and J. Sanllehí, "Application of thermoelectric generators for low-temperature-gradient energy harvesting," *Applied Sciences (Switzerland)*, vol. 13, 2 2023.
- [10] J. Curry, M. Specht, Z. Feng, A. Komolafe, C. Craig, D. Hewak, N. Harris, I. Zeimpekis, and K. A. Morgan, "Ot10.125 - harvesting body temperature to power wearable systems using sputtered flexible thermoelectrics," in *Lectures*. AMA Service GmbH, Von-Münchhausen-Str. 49, 31515 Wunstorf, 2024, pp. 213–214. [Online]. Available: <https://www.ama-science.org/doi/10.5162/EUROSENSORSXXXVI/OT10.125>

- [11] "Cubesat design specification rev. 14.1," Cal Poly, Tech. Rep., 2022.
- [12] B. Foing, L. Eurospacehub, and L. Observatory, "Why space exploration will be soon unsustainable, without a serious civilian space settlement programme," International Astronautical Congress, Tech. Rep., 10 2021. [Online]. Available: <https://www.researchgate.net/publication/355793424>
- [13] J. May, "Next in space 2025," 4 2025. [Online]. Available: <https://www.pwc.com/us/en/industries/industrial-products/library/space-industry-trends.html>
- [14] S. Blair, "9 space stations of the future that will carry the baton once the international space station is deorbited," *BBC Sky at Night Magazine*, 7 2024. [Online]. Available: <https://www.skyatnightmagazine.com/space-missions/future-space-stations-replace-iss>
- [15] "Most people in orbit at the same time," 2024. [Online]. Available: https://www.guinnessworldrecords.com/world-records/775645-most-people-in-orbit-at-the-same-time?utm_source=chatgpt.com
- [16] M. J. Heikens, A. M. Gorbach, H. S. Eden, D. M. Savastano, K. Y. Chen, M. C. Skarulis, and J. A. Yanovski, "Core body temperature in obesity," *American Journal of Clinical Nutrition*, vol. 93, pp. 963–967, 5 2011.
- [17] V. S. Koscheyev and G. R. Leon, *Spacesuits: Development and design for thermal comfort*. Elsevier Inc., 8 2014, pp. 171–191.
- [18] M. V. Ehrenfried, *Stratonauts: Pioneers Venturing into the Stratosphere*. Springer International Publishing, 2014.
- [19] H. J. McMann and K. S. Thomas, *U.S. Spacesuits*, 2nd ed. Springer New York, 2006.
- [20] "Why do we really need pressure suits?" pp. 9–9, 2023. [Online]. Available: <https://www.nasa.gov/wp-content/uploads/2023/05/dressing-for-altitude-nov-2017.pdf>
- [21] J. W. Wilson, B. M. Anderson, F. A. Cucinotta, J. Ware, and C. J. Zeitlin, "Spacesuit radiation shield design methods," Tech. Rep.
- [22] "Axemu technology & design," 10 2024. [Online]. Available: <https://brandfolder.com/axiomspace/newsroom/#!asset/qcqs7mpprb6mhpv3wp7wrg8>
- [23] "Testing of next-gen spacesuit underway," 1 2024. [Online]. Available: <https://www.axiomspace.com/news/axemu-spacesuit-testing>
- [24] "Gemini mission report - gemini iv (unclassified)," NASA, Tech. Rep., 12 1965. [Online]. Available: <https://ntrs.nasa.gov/api/citations/19670095754/downloads/19670095754.pdf>

- [25] "Apollo 17 mission report," NASA, Tech. Rep., 3 1973. [Online]. Available: https://www.nasa.gov/wp-content/uploads/static/history/alsj/a17/A17_MissionReport.pdf
- [26] Österreichisches Weltraum Forum News, "New spacesuits for the moon & beyond," 3 2013. [Online]. Available: <https://oewf.org/en/2023/03/new-spacesuits-for-the-moon-beyond/>
- [27] "History of spacesuits." [Online]. Available: <https://humans-in-space.jaxa.jp/en/life/wear-in-space/history/>
- [28] "Axiom suit — axiom space." [Online]. Available: <https://www.axiomspace.com/axiom-suit>
- [29] J. A. Jeevarajan and E. C. Darcy, "New lithium-ion polymer battery for the extravehicular mobility unit suit," Tech. Rep.
- [30] "Power: Radioisotope thermoelectric generators - nasa science." [Online]. Available: <https://science.nasa.gov/planetary-science/programs/radioisotope-power-systems/power-radioisotope-thermoelectric-generators/>
- [31] T. Cao, X. L. Shi, M. Li, B. Hu, W. Chen, W. D. Liu, W. Lyu, J. MacLeod, and Z. G. Chen, "Advances in bismuth-telluride-based thermoelectric devices: Progress and challenges," 6 2023.
- [32] M. D. Kadam, P. M. Gore, and B. Kandasubramanian, "Fiber-based thermoelectric generators and their substrate materials," *Hybrid Advances*, vol. 5, p. 100177, 4 2024.
- [33] J. F. Serrano-Claumarchirant, M. A. Nasiri, C. Cho, A. Cantarero, M. Culebras, and C. M. Gómez, "Textile-based thermoelectric generator produced via electrochemical polymerization," *Advanced Materials Interfaces*, vol. 10, 3 2023.
- [34] D. Yang, X. L. Shi, M. Li, M. Nisar, A. Mansoor, S. Chen, Y. Chen, F. Li, H. Ma, G. X. Liang, X. Zhang, W. Liu, P. Fan, Z. Zheng, and Z. G. Chen, "Flexible power generators by ag₂se thin films with record-high thermoelectric performance," *Nature Communications*, vol. 15, 12 2024.
- [35] N. Kuang, Z. Zuo, W. Wang, and R. Liu, "High performance flexible thin-film thermoelectric generator heated by methanol catalytic combustion," *Applied Thermal Engineering*, vol. 219, 1 2023.
- [36] J. Jing, L. Chopplet, N. Battaglini, V. Noël, B. Piro, T. Leydecker, Z. Wang, G. Mattona, and E. Orgiu, "The role of substrates and electrodes in inkjet-printed pedot:pss thermoelectric generators," *Journal of Materials Chemistry C*, vol. 12, pp. 6185–6192, 3 2024.

- [37] Y. Liu, Q. Zhang, A. Huang, K. Zhang, S. Wan, H. Chen, Y. Fu, W. Zuo, Y. Wang, X. Cao, L. Wang, U. Lemmer, and W. Jiang, "Fully inkjet-printed ag₂se flexible thermoelectric devices for sustainable power generation," *Nature Communications*, vol. 15, 12 2024.
- [38] T. Torfs, V. Leonov, and C. V. Hoof, "Body-heat powered autonomous pulse oximeter," Tech. Rep., 2006.
- [39] C. S. Kim, H. M. Yang, J. Lee, G. S. Lee, H. Choi, Y. J. Kim, S. H. Lim, S. H. Cho, and B. J. Cho, "Self-powered wearable electrocardiography using a wearable thermoelectric power generator," *ACS Energy Letters*, vol. 3, pp. 501–507, 3 2018.
- [40] K. A. Morgan, T. Tang, I. Zeimpekis, A. Ravagli, C. Craig, J. Yao, Z. Feng, D. Yarmolich, C. Barker, H. Assender, and D. W. Hewak, "High-throughput physical vapour deposition flexible thermoelectric generators," *Scientific Reports*, vol. 9, 12 2019.
- [41] L. E. Bell, "Cooling, heating, generating power, and recovering waste heat with thermoelectric systems," Tech. Rep. [Online]. Available: <https://www.science.org>
- [42] N. Jaziri, A. Boughamoura, J. Müller, B. Mezghani, F. Tounsi, and M. Ismail, "A comprehensive review of thermoelectric generators: Technologies and common applications," pp. 264–287, 12 2020.
- [43] L. Miao, S. Zhu, C. Liu, J. Gao, Z. Zhang, Y. Peng, J. L. Chen, Y. Gao, J. Liang, and T. Mori, "Comfortable wearable thermoelectric generator with high output power," *Nature communications*, vol. 15, p. 8516, 12 2024.
- [44] R. Merienne, J. Lynn, E. McSweeney, and S. M. O'Shaughnessy, "Thermal cycling of thermoelectric generators: The effect of heating rate," *Applied Energy*, vol. 237, pp. 671–681, 3 2019.
- [45] P. Wang, J. E. Li, B. L. Wang, T. Shimada, H. Hirakata, and C. Zhang, "Lifetime prediction of thermoelectric devices under thermal cycling," *Journal of Power Sources*, vol. 437, 10 2019.
- [46] W. Ding, X. Shen, M. Jin, Y. Hu, Z. Chen, E. Meng, J. Luo, W. Li, and Y. Pei, "Robust bendable thermoelectric generators enabled by elasticity strengthening," *Nature communications*, vol. 15, p. 9767, 12 2024.
- [47] W. Ren, Y. Sun, D. Zhao, A. Aili, S. Zhang, C. Shi, J. Zhang, H. Geng, J. Zhang, L. Zhang, J. Xiao, and R. Yang, "A p p l i e d s c i e n c e s a n d e n g i n e e r i n g high-performance wearable thermoelectric generator with self-healing, recycling, and lego-like reconfiguring capabilities," Tech. Rep., 2021. [Online]. Available: <https://www.science.org>

- [48] “Orbital elements of iss.” [Online]. Available: <https://in-the-sky.org/spacecraft-elements.php?id=25544>
- [49] G. Salazar-Salinas, E. Botello-Ramírez, and E. Avalos-Gauna, “Thermal analysis of a 3u-cubesat, a case study of pakal satellite,” in *International Conference on Fluid Flow, Heat and Mass Transfer*. Avestia Publishing, 2021.
- [50] N. Kiomarsipour, R. S. Razavi, and K. Ghani, “Improvement of spacecraft white thermal control coatings using the new synthesized zn-mcm-41 pigment,” *Dyes and Pigments*, vol. 96, pp. 403–406, 2 2013.
- [51] L. Kauder, “Spacecraft thermal control coatings references,” NASA Technical Reports, Tech. Rep., 12 2005. [Online]. Available: <https://ntrs.nasa.gov/search.jsp?R=20070014757>
- [52] R. M. Wakefield, “Surface emissivity of a reinforced carbon composite material with an oxidation-inhibiting coating,” Ames Research Center, Tech. Rep., 10 1973. [Online]. Available: <https://ntrs.nasa.gov/citations/19740004171>
- [53] ASM, *Properties and Selection: Nonferrous Alloys and Special-Purpose Materials*, 1990, vol. 2.
- [54] D. Lide, *CRC Handbook of Chemistry and Physics*, 84th ed. CRC Press LLC, 2004.
- [55] G. Thummerer, K.-H. Gresslehner, R. Sharif, and G. Hendorfer, “Characterization of commercial bi₂te₃ thermoelectric materials,” 01 2001.
- [56] “Earth albedo and emitted radiation,” NASA, Tech. Rep., 7 1971. [Online]. Available: <https://ntrs.nasa.gov/api/citations/19710023628/downloads/19710023628.pdf>
- [57] K. Lowe, “Applying human rating to the nasa-std-3001: An overview,” 8 2025. [Online]. Available: <https://www.nasa.gov/human-rating-guidance/>

Appendix A

AI Declaration Form

GenAI Declaration Form

Name	Student ID
Matthew Enfield	36606782
Module Code	Assignment name / description
FEEG6012	MSc Research Project
Have you used GenAI? (Tick for yes)	<input checked="" type="checkbox"/>
Date: 10/09/2025	
Which GenAI tools have you used? (Include version / leave blank if not used)	
Grok 3	

Standard declaration:

For each GenAI use (see definitions and codes over the page), summarise which questions and how each was used (suggest 1 or 2 sentences per use category)
A1: I learnt basic COMSOL Multiphysics skills such as building geometry and importing physics
A2: AI gave me a summary of recent developments of thermoelectric technology

Academic Conduct

I acknowledge I have answered honestly on this declaration form	<input checked="" type="checkbox"/>
I understand if I was unsure about whether my actions met academic conduct requirements, it is my responsibility to confirm with the teaching team prior to submission	<input checked="" type="checkbox"/>
I am aware of and have critically reviewed the content generated by GenAI used in this submission. I accept responsibility for this content and can be asked about it in the future	<input checked="" type="checkbox"/>

FIGURE A.1: AI Declaration Form